Dissipative Dynamics of a Driven Quantum Spin Coupled to a Bath of Ultracold Fermions

Dissipative dynamics of a driven quantum spin coupled to a bath of ultracold fermions

Michael Knap,[1,2] Dmitry A. Abanin,[1,3] and Eugene Demler[1]

[1] *Department of Physics, Harvard University, Cambridge MA 02138, USA*
[2] *ITAMP, Harvard-Smithsonian Center for Astrophysics, Cambridge, MA 02138, USA*
[3] *Perimeter Institute for Theoretical Physics, Waterloo, N2L2Y5 ON, Canada*

(Dated: January 6, 2014)

We explore the dynamics and the steady state of a driven quantum spin coupled to a bath of fermions, which can be realized with a strongly imbalanced mixture of ultracold atoms using currently available experimental tools. Radio-frequency driving can be used to induce tunneling between the spin states. The Rabi oscillations are modified due to the coupling of the quantum spin to the environment, which causes frequency renormalization and damping. The spin-bath coupling can be widely tuned by adjusting the scattering length through a Feshbach resonance. When the scattering potential creates a bound state, by tuning the driving frequency it is possible to populate either the ground state, in which the bound state is filled, or a metastable state in which the bound state is empty. In the latter case, we predict an emergent inversion of the steady-state magnetization. Our work shows that different regimes of dissipative dynamics can be explored with a quantum spin coupled to a bath of ultracold fermions.

PACS numbers: 47.70.Nd, 67.85.-d, 71.10.Pm, 72.10.-d

Ultracold atomic systems provide a versatile laboratory to explore real-time many-body dynamics due to their long coherence times and tunability [1, 2] and, in particular, to study rich impurity physics [3–10]. In recent years, much progress has been achieved in realizing quantum impurities interacting with many-body environments. Examples include quantum degenerate gases consisting of a single atom type, where a few atoms are transferred to a different hyperfine state [11–15], ions immersed in quantum gases [16–18], and strongly imbalanced mixtures of multiple atomic species [19–22]. Impurity atoms generally have several hyperfine states that interact differently with the host particles. Coherent control of these states allows one to probe the influence of environmental coupling on impurity dynamics, e.g. in Fermi polarons, which are impurities dressed by particle-hole pairs [23–27]. So far experimental studies focused mostly on the spectral properties [11, 20, 21] and mass renormalization [12, 14] of polarons. However, very recently Rabi oscillations of moving quantum spins, encoded in two hyperfine states of the impurity atoms, have been explored [20], which gave further insights into polaron dynamics.

Inspired by the tremendous experimental progress, here we analyze the dynamics of a quantum spin interacting with an ultracold fermionic bath (Fig. 1 (a)–(b)). We consider a situation where the spin performs radio-frequency (RF) driven Rabi oscillations, and study their frequency renormalization and damping due to spin-bath interactions. We find that this system realizes various regimes of dissipative dynamics. Moreover, we predict an emergent inversion of the steady-state magnetization when the scattering potential creates a bound state yet the driving is tuned to a metastable state in which the bound state remains unoccupied.

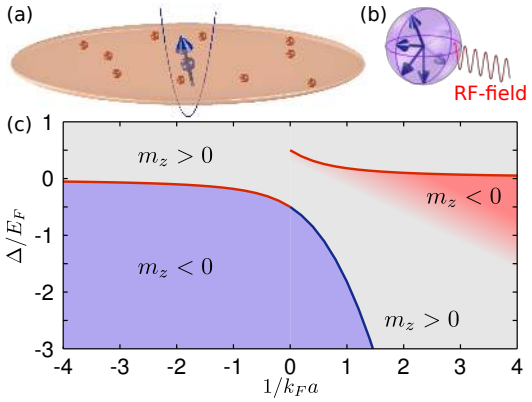

FIG. 1. (Color online) (a) A driven quantum spin, which is dissipatively coupled to a bath of fermions, can be experimentally realized with localized impurity atoms (sphere with arrow) that are immersed in a Fermi gas (small spheres). (b) Two hyperfine states of the impurities are driven by RF fields of strength Ω_0 detuned from the bare transition by Δ. (c) The sign of the steady-state magnetization m_z of the driven quantum spin is shown as a function of inverse scattering length $1/k_F a$ and detuning Δ/E_F. Along the solid lines m_z vanishes and non-trivial powerlaw frequency renormalizations and damping of the Rabi oscillations are found. A transition from normal $m_z > 0$ to inverted $m_z < 0$ magnetization emerges below the metastable state, red shaded area.

We consider an experimentally relevant situation where the host fermions interact with the impurity via contact interactions, such that only s-wave scattering is important. Without loss of generality, we assume that only one of the spin states, $|\uparrow\rangle$, interacts with host fermions with scattering length a, while the other, $|\downarrow\rangle$, does not. This scenario has been experimentally realized e.g. in [20, 21]. We mostly focus on the case when

the quantum spin can be treated as immobile (this is true when the impurity is localized by a strong potential [28] or is very heavy compared to host fermions). Two cases should be distinguished: (1) $a < 0$, when the impurity potential does not create a bound state, and (2) $a > 0$, when a bound state exists [29, 30]. We show below through analytic arguments and numerical simulations that in both cases, in the low-energy limit, our problem maps onto the spin-boson model with an ohmic bath, characterized by the low-energy spectral density $J(\omega) = 2\alpha\omega$ [31–33] where α is the dimensionless coupling strength, that is widely tunable by changing the scattering length a. Further, the energy difference between the two states in the spin-boson model is controlled by the frequency of the driving field.

In case (1), $a < 0$, the dissipative coupling can be related to the scattering phase shift at the Fermi level, $\delta_F = -\tan^{-1}(k_F a)$, via

$$\alpha_1 = \frac{\delta_F^2}{2\pi^2}\,. \tag{1}$$

Even richer is case (2), $a > 0$, where depending on the driving frequency, the physics of the driven quantum spin is governed by effective spin-boson models with two different couplings. When the driving frequency is such that the bound state is populated during the Rabi oscillations, the coupling constant of the equivalent spin-boson model is

$$\alpha_2 = \frac{(\delta_F/\pi + 1)^2}{2}. \tag{2}$$

It is, however, also possible to tune the frequency to a *metastable* state with unoccupied bound state. In that case, the coupling constant of the equivalent spin-boson model is given by α_1, as in case (1). This allows one to explore a much broader range of coupling parameters, and, in particular, to approach the overdamped regime [31]. Further, the dissipative phase transition of the spin-boson model at $\alpha = 1$ [31] can be explored with a multi-component Fermi bath.

Model.—Our system is described by an effective one-dimensional Hamiltonian

$$\hat{H} = \hat{H}_0 + |\uparrow\rangle\langle\uparrow| \otimes \hat{V} + \Omega_0\hat{\sigma}_x - \Delta\hat{\sigma}_z\,, \tag{3}$$

where $\hat{H}_0 = \sum_k \epsilon_k c_k^\dagger c_k$ is the Hamiltonian of the host fermions and $\hat{V} = \frac{V}{L}\sum_{k,q} c_k^\dagger c_q$ is the contact impurity scattering potential. The last two terms of Eq. (3) model the RF driving of the two impurity spin states $|\downarrow\rangle$, $|\uparrow\rangle$. The parameters Ω_0 and Δ represent the tunneling amplitude between two spin states and the detuning, and can be independently controlled in experiment by changing the strength and frequency of the RF field. We will be interested in the situation where at $t < 0$ the spin is in the $|\downarrow\rangle$ state, and fermions are in the ground state $|\mathrm{FS}\rangle$. The driving is turned on at $t = 0$. We will explore how the populations of the two spin states, $n_\sigma := \langle\hat{n}_\sigma(t)\rangle$, $\sigma \in \{\downarrow, \uparrow\}$, which are readily accessible in experiments, evolve with time.

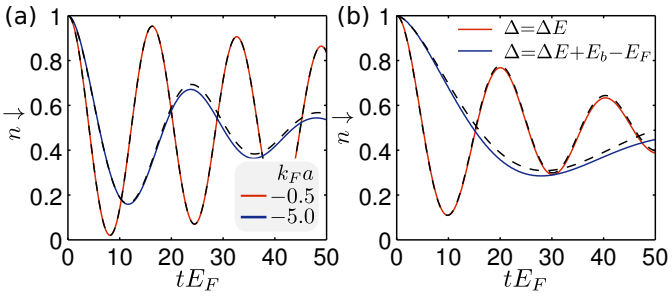

FIG. 2. (Color online) Time dependent occupation $n_\downarrow$ of the state $|\downarrow\rangle$ at resonance $\epsilon = 0$ for driving strength $\Omega_0 = 0.1E_F$. The Rabi oscillations are strongly damped and their frequencies renormalized. (a) $n_\downarrow$ for negative scattering length $k_F a = \{-0.5, -5.0\}$. (b) $n_\downarrow$ for the positive scattering length $k_F a = 2$ and RF field tuned to $\Delta = \Delta E$ and to $\Delta = \Delta E + E_b - E_F$, respectively. In all cases the steady-state magnetization is zero. Solid lines are numerical results from the simulation of (3) and dashed lines are obtained from perturbation theory.

Relation to spin-boson model.—In order to establish a low-energy description of our model for the case $a < 0$ (no bound state), we bosonize Hamiltonian (3) [4, 34–37] and find

$$\hat{H} = \sum_q v_F|q|b_q^\dagger b_q + \sqrt{2\alpha_1}\pi v_F\sum_{q>0}\left(\frac{q}{2\pi L}\right)^{1/2}(b_q^\dagger + b_q)\hat{\sigma}_z + \Omega_0\hat{\sigma}_x + \epsilon\hat{\sigma}_z\,, \tag{4}$$

which corresponds to the spin-boson model with an ohmic bath and dimensionless coupling α_1. Eq. (1) relates α_1 to the parameters of the microscopic model.

The energy of the $|\uparrow\rangle$ state is renormalized by the interactions with the Fermi sea (3) [38]:

$$\Delta E = -\int_0^{E_F}\frac{dE}{\pi}\delta(\sqrt{2mE}), \tag{5}$$

where m is the mass of host atoms and E_F is the Fermi energy. Thus, the two families of states, one involving the $|\downarrow\rangle$ state and the other the $|\uparrow\rangle$ state, become effectively degenerate when the detuning compensates the energy renormalization, i.e., $\Delta = \Delta E$. Generally, the energy difference is $\epsilon = -\Delta + \Delta E$, which describes the effective bias of the quantum spin. The effective bias ϵ, determines the steady-state magnetization $m_z := \lim_{t\to\infty}\{\langle\hat{n}_\uparrow(t)\rangle - \langle\hat{n}_\downarrow(t)\rangle\}$ [39, 40], whose sign we plot in Fig. 1 (c) as a function of the detuning Δ and the scattering length a. For $\epsilon = 0$, i.e. along the solid red line, $m_z = 0$.

For $a > 0$, the situation is more involved, because of the presence of the bound state whose population dynamics influences the oscillations of the quantum spin. The oscillations occur between two families of states, one

with the quantum spin in the $|\downarrow\rangle$ state and the other with the quantum spin in the $|\uparrow\rangle$ state. Our finding is that the latter can be either the ground state of the spin-up sector $|\Psi^g_\uparrow\rangle$ in which the bound state is occupied, or the metastable state $|\Psi^m_\uparrow\rangle$ in which the bound state is empty.

In order to understand the two regimes and their properties, it is instructive to consider the correlation function $F(t) = \langle\Psi_\downarrow|e^{-i\hat{H}t}|\Psi_\downarrow\rangle$. It should be noted that $F(t)$ determines spectral, rather than dynamical properties, yet, it will give us useful intuition. Following Yuval and Anderson [41, 42], $F(t)$ can be represented as a perturbative series in Ω_0, where at order n the spin flips n times at times $t_1, t_2, \ldots t_n$. This reduces the problem to understanding the response of the Fermi gas to a potential introduced at $t_1, t_3, \ldots t_n$. In the absence of the bound state, such responses have a characteristic form of a Cauchy determinant [41]. The only parameter that enters those expressions is α_1. To obtain $F(t)$, one then should sum over different spin flip times.

When the impurity potential creates a bound state, the response of the Fermi gas for a given spin trajectory contains different contributions, coming from the intermediate states in which the bound state is either filled or empty. However, when detuning is such that $|\Psi_\downarrow\rangle$ is resonant with either the metastable $|\Psi^m_\uparrow\rangle$ or the ground state $|\Psi^g_\uparrow\rangle$, the contributions from intermediate states of one kind would dominate. Contributions of the other kind will oscillate rapidly (due to the large energy difference involved) and therefore, upon integration, their contribution will become negligible.

For the case of only one spin flip, when the response function corresponds to the Anderson orthogonality catastrophe [43–45] it is known that both contributions have a similar power-law form, but with different exponents. The first contribution (empty bound state) is characterized by an exponent $2\alpha_1$, while the second one (filled bound state) by $2\alpha_2$. Generalizing this to the case of many spin flips, one can show, by extending the analysis of Combescot and Nozières [29], that the second contribution has the same form as the first one, but with exponent $2\alpha_2$. Thus, $F(t)$ is characterized by either α_1 or α_2 depending on the resonance condition.

The above argument strongly suggests that, effectively, our model becomes equivalent to the spin-boson model with coupling α_2 when $\Delta = \Delta E + E_b - E_F$, E_b being the bound state energy, [blue line in Fig. 1 (c)] and with α_1 when $\Delta = \Delta E$, [red line in Fig. 1 (c)]. To substantiate this expectation, we performed numerical simulations of the spin dynamics of Hamiltonian (3) using matrix product states (MPS), where the initial ground state of the system is determined by density matrix renormalization group [46, 47]. The time evolution with switched-on driving field is calculated with time evolving block decimation [48, 49]. We choose in (3) the dispersion of a one-dimensional lattice $\epsilon_k = -2J\cos k$ at half filling [50], for which we find the relation $-k_F a = V/v_F$ by comparing the scattering phase shift of the lattice and the continuum. We measure the occupation of the hyperfine states $\hat{n}_\downarrow$ and $\hat{n}_\uparrow$, respectively, from which we extract the renormalized Rabi frequency as well as damping by fitting to a damped, harmonic oscillator superimposed with a linear slope [37].

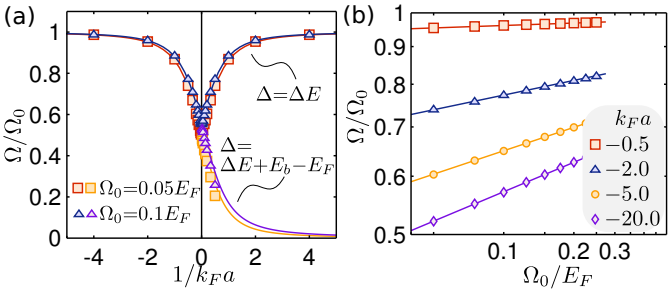

FIG. 3. (Color online) Powerlaw renormalization of the dressed Rabi frequency Ω_0 at resonance $\epsilon = 0$ due to coupling to the bath. (a) Dressed Rabi frequency Ω/Ω_0 as a function of the inverse scattering length $1/k_F a$ for two different driving field strengths $\Omega_0 = 0.05E_F$ and $\Omega_0 = 0.1E_F$. (b) Scaling of Ω/Ω_0 as a function of Ω_0 for different values of the interaction strength $k_F a$. The data is shown on a double logarithmic scale. The numerical results (symbols) are well described by analytic formula (6) (solid lines).

Driving at resonance ($\epsilon = 0$)**.**—We first consider zero effective detuning $\epsilon = 0$ and thus follow the solid lines in Fig. 1 (c), where $m_z = 0$. The numerically calculated time evolution of $n_\downarrow$ for driving strength $\Omega_0 = 0.1E_F$, negative scattering length $a < 0$, and $\Delta = \Delta E$ is shown in Fig. 2 (a), solid lines. With increasing interaction strength $|k_F a|$, the Rabi frequency Ω is strongly reduced while the damping rate γ is enhanced. $n_\downarrow$ is shown in (b) for positive scattering length $k_F a = 2$ but different values of the detuning $\Delta = \Delta E$ and $\Delta = \Delta E + E_b - E_F$. When tuning to the bound state branch the dressed Rabi frequency decreases significantly, illustrating that the coupling α increases due to the increase of scattering phase shift by π.

To confirm the equivalence of the dynamics to that of the spin-boson model, we fit the numerical data by the analytical results obtained from noninteracting blip approximation (NIBA), which is a weak coupling expansion valid for $\alpha \ll 1/2$ and at short times [31, 51]. Under NIBA the dynamics is divided into coherent and incoherent contributions. The coherent part consists of dressed Rabi oscillations of frequency Ω with a superimposed exponential damping γ which are universally related through $\Omega/\gamma = -\tan\pi/(2-2\alpha)$. The dressed Rabi frequency Ω can be expressed as [31]

$$\frac{\Omega}{\Omega_0} = F(\alpha)\left(\frac{\Omega_0}{\omega_c}\right)^{\frac{\alpha}{1-\alpha}}, \qquad (6)$$

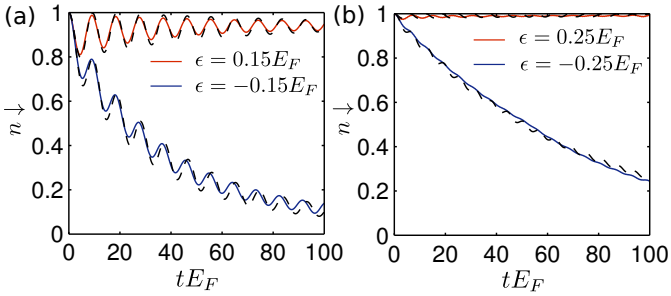

FIG. 4. (Color online) Time dependent occupation $n_\downarrow$ off resonance $\epsilon \neq 0$ for a driving strength $\Omega_0 = 0.1E_F$ and scattering length (a) $k_F a = -2$ and (b) $k_F a = 2$. For the latter the detuning is chosen with respect to the metastable branch. Solid lines are numerical and dashed lines perturbative results.

with $F(\alpha) := [\Gamma(1-2\alpha)\cos(\pi\alpha)]^{\frac{1}{2(1-\alpha)}} \sin\frac{\pi}{2(1-\alpha)}$ and ω_c is the high energy cutoff of the spin-boson theory. For $\Omega_0 < \omega_c$ this equation gives a *reduction* of the dressed Rabi frequency Ω as compared to the driving strength Ω_0. The dashed curves in Fig. 2 are obtained from NIBA with the high energy cutoff as the only fitting parameter. For small interaction and at short to medium time scales NIBA describes the dynamics well.

We extracted the renormalization of the Rabi frequency for several values of interaction strength and detuning for $\Omega_0 = 0.05E_F$ and $\Omega_0 = 0.1E_F$, Fig. 3 (a). The branch present for both positive and negative values of scattering length is obtained by setting $\Delta = \Delta E$, while the second branch at $a > 0$ is obtained with $\Delta = \Delta E + E_b - E_F$. For small positive $k_F a$ the driving cannot couple effectively to the bound state as its wavefunction is of small spatial extend; hence for the ground state branch symbols are shown for $k_F a \gtrsim 1$. The powerlaw renormalization (6) of the dressed Rabi frequency is demonstrated in Fig. 3 (b). Thus we can conclude that the dynamics of our system is well-described by an effective spin-boson model for both positive and negative scattering length.

Driving off resonance ($\epsilon \neq 0$).—The case of off-resonant driving ($\epsilon \neq 0$) effectively corresponds to a biased spin-boson model. Depending on the sign of ϵ, the quantum spin has either positive or negative steady-state magnetization m_z, Fig. 1 (c).

In Fig. 4 the numerically evaluated time-dependent occupation $n_\downarrow$, solid lines, is shown for $\Omega_0 = 0.1E_F$, effective detuning $\epsilon = \pm 0.15E_F$, and (a) $k_F a = -2$ and (b) $k_F a = 2$. These numerical results are compared to a weak coupling expansion to first order in the blip-blip interaction [39, 40], dashed lines. For negative scattering length (a) and $\epsilon > 0$ a quantum spin prepared in $|\downarrow\rangle$ decoheres only weakly; in agreement with $m_z < 0$, Fig. 1 (c). For $\epsilon < 0$ ($m_z > 0$), the occupation slowly flips with a rate that is indirect proportional to the detuning. In (b) the system is slightly detuned from the metastable branch. For $\epsilon < 0$ the magnetization slowly reverts from negative to positive, indicating $m_z > 0$, while for $\epsilon > 0$, the $|\downarrow\rangle$ state remains highly occupied over long times, supporting the region of inverted magnetization below the metastable branch shown in Fig. 1 (c).

Summary and discussion.—We studied the dynamics of a driven quantum spin coupled to a fermionic bath which can be realized with an imbalanced mixture of ultracold atoms. Two hyperfine-states of the minority atoms serve as spin states and atoms themselves are spatially localized by a strong optical lattice [28]. We used the mapping to the spin-boson model to study the problem analytically. For the unbiased case ($\epsilon = 0$), the spin-boson model exhibits a dissipative phase transition at coupling $\alpha = 1$ [31–33]. With a single component bath, the coupling can take values (1) $0 < \alpha_1 < 1/8$ and (2) $1/8 < \alpha_2 < 1/2$. For $a < 0$ range (1) can be explored, while for $a > 0$ both ranges are accessible. To explore an even broader range of α, one may consider an impurity immersed in a multi-component Fermi gas. Such gases can e.g. be realized with alkaline-earth atoms [52–54] that obey SU(N) symmetry for which the coupling constant is enhanced by N compared to the single-channel case. Thus, for $N > 2$ it should be possible to explore the dissipative phase transition.

Qualitatively, the existence of two resonances is reminiscent of experiments [20, 21], which studied mobile impurities interacting with a three-dimensional Fermi gas. In this case, at $a > 0$ stable and metastable polaron branches have been observed. Moreover, authors of Ref. [20] experimentally studied Rabi oscillations of the impurity spin at resonance. It should be noted, however, that for a mobile impurity, effectively, the Fermi gas provides a sub-ohmic, rather than ohmic bath. In this case the effect of the bath is generally described by damping, and no dissipative phase transition exists [31]. It is possible, however, that at short times, and for heavy impurities (as was the case in Ref. [20]), our results will still be applicable at least qualitatively.

The authors thank G.M. Bruun and E.G. Dalla Torre for useful discussions and M. Ganahl for providing his MPS code [55]. The authors acknowledge support from Harvard-MIT CUA, the DARPA OLE program, AFOSR MURI on Ultracold Molecules, ARO-MURI on Atomtronics, as well as the Austrian Science Fund (FWF) Project No. J 3361-N20. Numerical simulations have been performed on the Vienna Scientific Cluster.

[1] I. Bloch, J. Dalibard, and W. Zwerger, Rev. Mod. Phys. **80**, 885 (2008)
[2] W. Ketterle and M. W. Zwierlein, in *Proceedings of the International School of Physics Enrico Fermi, Course CLXIV*, edited by M. Inguscio, W. Ketterle, and C. Sa-

lomon (2008)
[3] A. Micheli, A. J. Daley, D. Jaksch, and P. Zoller, Phys. Rev. Lett. **93**, 140408 (2004)
[4] A. Recati, P. O. Fedichev, W. Zwerger, J. von Delft, and P. Zoller, Phys. Rev. Lett. **94**, 040404 (2005)
[5] M. Bruderer and D. Jaksch, New J. Phys. **8**, 87 (2006)
[6] M. B. Zvonarev, V. V. Cheianov, and T. Giamarchi, Phys. Rev. Lett. **99**, 240404 (2007)
[7] A. Lamacraft, Phys. Rev. Lett. **101**, 225301 (2008)
[8] S. Lal, S. Gopalakrishnan, and P. M. Goldbart, Phys. Rev. B **81**, 245314 (2010)
[9] P. P. Orth, D. Roosen, W. Hofstetter, and K. Le Hur, Phys. Rev. B **82**, 144423 (2010)
[10] P. P. Orth, A. Imambekov, and K. Le Hur, Phys. Rev. A **82**, 032118 (2010)
[11] A. Schirotzek, C. Wu, A. Sommer, and M. W. Zwierlein, Phys. Rev. Lett. **102**, 230402 (2009)
[12] S. Nascimbène, N. Navon, K. J. Jiang, L. Tarruell, M. Teichmann, J. McKeever, F. Chevy, and C. Salomon, Phys. Rev. Lett. **103**, 170402 (2009)
[13] S. Palzer, C. Zipkes, C. Sias, and M. Köhl, Phys. Rev. Lett. **103**, 150601 (2009)
[14] N. Navon, S. Nascimbène, F. Chevy, and C. Salomon, Science **328**, 729 (2010)
[15] T. Fukuhara, A. Kantian, M. Endres, M. Cheneau, P. Schau, S. Hild, D. Bellem, U. Schollwöck, T. Giamarchi, C. Gross, I. Bloch, and S. Kuhr, Nat. Phys. **9**, 235 (2013)
[16] C. Zipkes, S. Palzer, C. Sias, and M. Köhl, Nature **464**, 388 (2010)
[17] S. Schmid, A. Härter, and J. H. Denschlag, Phys. Rev. Lett. **105**, 133202 (2010)
[18] L. Ratschbacher, C. Sias, L. Carcagni, J. M. Silver, C. Zipkes, and M. Köhl, Phys. Rev. Lett. **110**, 160402 (2013)
[19] S. Will, T. Best, S. Braun, U. Schneider, and I. Bloch, Phys. Rev. Lett. **106**, 115305 (2011)
[20] C. Kohstall, M. Zaccanti, M. Jag, A. Trenkwalder, P. Massignan, G. M. Bruun, F. Schreck, and R. Grimm, Nature **485**, 615 (2012)
[21] M. Koschorreck, D. Pertot, E. Vogt, B. Fröhlich, M. Feld, and M. Köhl, Nature **485**, 619 (2012)
[22] J. Catani, G. Lamporesi, D. Naik, M. Gring, M. Inguscio, F. Minardi, A. Kantian, and T. Giamarchi, Phys. Rev. A **85**, 023623 (2012)
[23] C. Lobo, A. Recati, S. Giorgini, and S. Stringari, Phys. Rev. Lett. **97**, 200403 (2006)
[24] F. Chevy, Phys. Rev. A **74**, 063628 (2006)
[25] F. Chevy and C. Mora, Rep. Prog. Phys. **73**, 112401 (2010)
[26] R. Schmidt and T. Enss, Phys. Rev. A **83**, 063620 (2011)
[27] P. Massignan and G. M. Bruun, Eur. Phys. J. D **65**, 83 (2011)
[28] Distinct species of atoms can have different polarizabilities, which allows to create an optical lattice that spatially confines one species without affecting the other [1, 56]; for a recent demonstration see, e.g. [22].
[29] M. Combescot and P. Nozières, J. Phys. France **32**, 913 (1971)
[30] M. Knap, A. Shashi, Y. Nishida, A. Imambekov, D. A. Abanin, and E. Demler, Phys. Rev. X **2**, 041020 (2012)
[31] A. J. Leggett, S. Chakravarty, A. T. Dorsey, M. P. A. Fisher, A. Garg, and W. Zwerger, Rev. Mod. Phys. **59**, 1 (1987)
[32] G. Schön and A. Zaikin, Phys. Rep. **198**, 237 (1990)
[33] M. Vojta, Phil. Mag. **86**, 1807 (2006)
[34] K. D. Schotte and U. Schotte, Phys. Rev. **182**, 479 (1969)
[35] F. Guinea, V. Hakim, and A. Muramatsu, Phys. Rev. B **32**, 4410 (1985)
[36] T. Giamarchi, *Quantum Physics in One Dimension* (Oxford University Press, USA, 2004)
[37] See Supplemental Material for theoretical derivations and numerical values.
[38] I. Affleck, Nucl. Phys. Proc. Suppl. **58**, 35 (1997)
[39] U. Weiss and M. Wollensak, Phys. Rev. Lett. **62**, 1663 (1989)
[40] R. Görlich, M. Sassetti, and U. Weiss, Europhys. Lett. **10**, 507 (1989)
[41] P. W. Anderson and G. Yuval, Phys. Rev. Lett. **23**, 89 (1969)
[42] G. Yuval and P. W. Anderson, Phys. Rev. B **1**, 1522 (1970)
[43] G. D. Mahan, Phys. Rev. **163**, 612 (1967)
[44] P. W. Anderson, Phys. Rev. Lett. **18**, 1049 (1967)
[45] P. Nozières and C. T. De Dominicis, Phys. Rev. **178**, 1097 (1969)
[46] S. R. White, Phys. Rev. Lett. **69**, 2863 (1992)
[47] U. Schollwöck, Rev. Mod. Phys. **77**, 259 (2005)
[48] G. Vidal, Phys. Rev. Lett. **91**, 147902 (2003)
[49] G. Vidal, Phys. Rev. Lett. **93**, 040502 (2004)
[50] This is similar to a continuum potential with effective range, which has also been considered to describe experiment [20].
[51] Finding exact solutions of the dynamics of the spin-boson beyond weak-coupling is subject of current research interest, see e.g. [57–61] and references therein. However, for our purpose a comparison to NIBA is sufficient.
[52] T. Fukuhara, Y. Takasu, M. Kumakura, and Y. Takahashi, Phys. Rev. Lett. **98**, 030401 (2007)
[53] S. Taie, Y. Takasu, S. Sugawa, R. Yamazaki, T. Tsujimoto, R. Murakami, and Y. Takahashi, Phys. Rev. Lett. **105**, 190401 (2010)
[54] S. Taie, R. Yamazaki, S. Sugawa, and Y. Takahashi, Nat. Phys. **8**, 825 (2012)
[55] M. Ganahl, E. Rabel, F. H. L. Essler, and H. G. Evertz, Phys. Rev. Lett. **108**, 077206 (2012)
[56] R. Grimm, M. Weidemüller, and Y. B. Ovchinnikov, Adv. At. Mol. Opt. Phys. **42**, 95 (2000)
[57] F. B. Anders, R. Bulla, and M. Vojta, Phys. Rev. Lett. **98**, 210402 (2007)
[58] P. P. Orth, A. Imambekov, and K. Le Hur, Phys. Rev. B **87**, 014305 (2013)
[59] D. M. Kennes, O. Kashuba, M. Pletyukhov, H. Schoeller, and V. Meden, Phys. Rev. Lett. **110**, 100405 (2013)
[60] O. Kashuba and H. Schoeller, Phys. Rev. B **87**, 201402(R) (2013)
[61] B. Sbierski, M. Hanl, A. Weichselbaum, H. E. Türeci, M. Goldstein, L. I. Glazman, J. von Delft, and A. İmamoğlu, Phys. Rev. Lett. **111**, 157402 (2013)

Supplemental material for: Dissipative dynamics of a driven quantum spin coupled to a bath of ultracold fermions

Bosonization of the Hamiltonian

Here, we provide details on the bosonization of Hamiltonian (3). The low-energy description for the free fermion part is [36]

$$\hat{H}_0 = \sum_k \epsilon_k c_k^\dagger c_k \to \sum_k v_F k (c_{kR}^\dagger c_{kR} - c_{kL}^\dagger c_{kL}) = \sum_k v_F k (c_{kR}^\dagger c_{kR} + c_{-kL}^\dagger c_{-kL}) \,, \tag{7}$$

where we introduced left (L) and right (R) movers. We now consider new particles by performing the canonical transformation

$$a_{kR} = \frac{1}{\sqrt{2}}(c_{kR} + c_{-kL}) \tag{8a}$$

$$a_{kL} = \frac{1}{\sqrt{2}}(-c_{kR} + c_{-kL}) \,. \tag{8b}$$

These new particles are fermions as they obey the respective anticommutation relations. Using the transformation Eq. (8), the free Hamiltonian reads

$$\hat{H}_0 \to \sum_k v_F k (a_{kR}^\dagger a_{kR} + a_{kL}^\dagger a_{kL}) \,, \tag{9}$$

which can be expressed as

$$\hat{H}_0 \to \frac{v_F}{2\pi} \int dx (\nabla\theta)^2 + (\nabla\phi)^2 = \sum_q v_F |q| b_q^\dagger b_q \,. \tag{10}$$

using the standard bosonization prescription [36].

The transformation (8) combines positive and negative momenta of the original fermions. Therefore, it would not be useful if generic quartic interactions were present in the Hamiltonian as those would be non-local in the new operators [36]. For our model, however, one finds that the interaction part between the fermions and the impurity couples only to the new right moving fermions

$$\begin{aligned} \hat{V} = \frac{V}{L} \sum_{k,q} c_k^\dagger c_q \to & \frac{V}{L} \sum_{k,q} (c_{kR}^\dagger + c_{kL}^\dagger)(c_{qR} + c_{qL}) = \frac{2V}{L} \sum_{k,q} a_{kR}^\dagger a_{kR} \\ & = -2V \frac{\nabla\phi_h(0)}{\pi} = -2V \sum_{q>0} \left(\frac{q}{2\pi L}\right)^{1/2} (b_q^\dagger + b_q) \,. \end{aligned} \tag{11}$$

In the second line we made use of the fact that right moving particles with full degrees of freedom can be equivalently expressed as left and right moving particles with half as many degrees of freedom via the relation $a_R(x<0) = a_L(-x)$ [36]. To indicate that only half of the degree's of freedom have to be considered we added the subscript h to the field $\phi(x)$. The full interaction part thus transforms as

$$|\uparrow\rangle\langle\uparrow| \hat{V} \to -V(\hat{\sigma}_z + \hat{\mathbb{1}}) \frac{\nabla\phi_h(0)}{\pi} \,, \tag{12}$$

where $\hat{\sigma}_z$ is shifted by the identity, since in the fermionic model the interaction is proportional to $|\uparrow\rangle\langle\uparrow|$. The local forward scattering $-V\frac{\nabla\phi_h(0)}{\pi}$ can be removed by a transformation of the form

$$\tilde{\phi}_h(x) = \phi_h(x) - \frac{V}{v_F}\Theta(x) \,, \qquad \tilde{\phi}_{\bar{h}}(x) = \phi_{\bar{h}}(x) \,, \tag{13}$$

where Θ is the Heaviside step function. In Eq. (13) we transformed half of the degrees of freedom indicated by h while the other half $\bar{h}$ remains invariant. With that one finds for the low energy properties of Hamiltonian (3)

$$\begin{aligned}\hat{H} &\sim \frac{v_F}{2\pi}\int dx\left[(\nabla\theta)^2+(\nabla\phi)^2-\frac{2V}{v_F}(\hat{\sigma}_z+\hat{\mathbb{1}})\nabla\phi_h(x)\delta(x)\right]+\Omega_0\hat{\sigma}_x-\Delta\hat{\sigma}_z\\ &= \frac{v_F}{2\pi}\int dx\Big[(\nabla\theta)^2+(\nabla\tilde{\phi})^2+\frac{2V}{v_F}\nabla\tilde{\phi}_h(x)\delta(x)+\frac{V^2}{v_F^2}\delta(x)\\ &\qquad -\frac{2V}{v_F}(\hat{\sigma}_z+\hat{\mathbb{1}})\Big(\nabla\tilde{\phi}_h(x)\delta(x)+\frac{V}{v_F}\delta(x)\Big)\Big]+\Omega_0\hat{\sigma}_x-\Delta\hat{\sigma}_z\\ &= \frac{v_F}{2\pi}\int dx\Big[(\nabla\theta)^2+(\nabla\tilde{\phi})^2\Big]-V\hat{\sigma}_z\frac{\nabla\tilde{\phi}_h(0)}{\pi}+\Omega_0\hat{\sigma}_x\underbrace{-(\frac{V^2}{\pi v_F}+\Delta)}_{=\epsilon}\hat{\sigma}_z+\text{const.}\end{aligned}$$

In standard boson notation the Hamiltonian reads

$$\hat{H}=\sum_q v_F|q|b_q^\dagger b_q+V\sum_{q>0}\Big(\frac{q}{2\pi L}\Big)^{1/2}(b_q^\dagger+b_q)\hat{\sigma}_z+\Omega\hat{\sigma}_x+\epsilon\hat{\sigma}_z\ , \tag{14}$$

which corresponds to Eq. (4) in the main text when identifying

$$\alpha=\frac{V^2}{2\pi^2 v_F^2}\ . \tag{15}$$

We obtain the latter relation from comparison with the spectral-density of the spin-boson model [31]

$$J(\omega)=\sum_q\lambda_q^2\delta(\omega-v_F|q|)\ , \tag{16}$$

where λ_q describes the coupling to the bath. For an ohmic bath, the low-energy spectral function is of the form

$$J(\omega)=2\alpha\omega\ . \tag{17}$$

Comparing Eq. (14) with the spin-boson model [31], we find $\lambda_q=2V\left(\frac{q}{2\pi L}\right)^{1/2}$ for $q>0$ and $\lambda_q=0$ for $q<0$ and thus

$$J(\omega)=\frac{V^2}{\pi^2}\int_0^\infty dq\,q\,\delta(\omega-v_F|q|)=2\frac{V^2}{2\pi^2 v_F^2}\omega\ . \tag{18}$$

From Eqs. (17) and (18) we then find Eq. (15).

Numerical values

In Tab. I we list numerical values for the ground state energy E, the spin-bath coupling α_1, α_2, and the energy renormalization ΔE, $\Delta E+E_b-E_F$ as a function of the interaction strength V $(k_F a)$ obtained from the lattice model, which we simulate using matrix product states. The considered system consists of $L=200$ sites and $N=100$ particles.

TABLE I. Numerical values for the ground state energy E, the spin-bath coupling α_1, α_2, and the energy renormalization ΔE, $\Delta E + E_b - E_F$ as a function of the interaction strength V ($k_F a$).

V	$k_F a$	E	α_1	ΔE	α_2	$\Delta E + E_b - E_F$
0.00	0.00	-127.462	0.000			
0.10	-0.05	-127.413	0.000	0.0488		
0.20	-0.10	-127.367	0.001	0.0950		
0.30	-0.15	-127.323	0.001	0.1388		
0.40	-0.20	-127.282	0.002	0.1803		
0.45	-0.23	-127.262	0.002	0.2001		
0.50	-0.25	-127.243	0.003	0.2193		
0.60	-0.30	-127.206	0.004	0.2561		
0.70	-0.35	-127.171	0.006	0.2907		
0.80	-0.40	-127.139	0.007	0.3232		
0.90	-0.45	-127.108	0.009	0.3537		
1.00	-0.50	-127.080	0.011	0.3823		
1.20	-0.60	-127.028	0.015	0.4343		
1.40	-0.70	-126.982	0.019	0.4799		
1.60	-0.80	-126.942	0.023	0.5201		
1.80	-0.90	-126.906	0.027	0.5555		
2.00	-1.00	-126.875	0.031	0.5868		
4.00	-2.00	-126.696	0.062	0.7659		
6.00	-3.00	-126.622	0.079	0.8402		
10.00	-5.00	-126.558	0.096	0.9040		
14.00	-7.00	-126.530	0.103	0.9322		
20.00	-10.00	-126.508	0.110	0.9536		
40.00	-20.00	-126.483	0.117	0.9787		
60.00	-30.00	-126.475	0.120	0.9871		
100.00	-50.00	-126.468	0.122	0.9938		
-100.00	50.00	-226.468	0.122	-99.0062	0.128	1.0138
-60.00	30.00	-186.475	0.120	-59.0129	0.130	1.0204
-40.00	20.00	-166.483	0.117	-39.0213	0.133	1.0287
-20.00	10.00	-146.508	0.110	-19.0464	0.141	1.0533
-14.00	7.00	-140.530	0.103	-13.0678	0.149	1.0743
-10.00	5.00	-136.558	0.096	-9.0960	0.158	1.1020
-6.00	3.00	-132.622	0.079	-5.1598	0.181	1.1648
-4.00	2.00	-130.696	0.062	-3.2341	0.210	1.2380
-2.00	1.00	-128.875	0.031	-1.4132	0.281	1.4152
-1.80	0.90	-128.706	0.027	-1.2445	0.294	1.4462
-1.60	0.80	-128.542	0.023	-1.0799	0.308	1.4814
-1.40	0.70	-128.382	0.019	-0.9201	0.324	1.5213
-1.20	0.60	-128.228	0.015	-0.7657	0.343	1.5667
-1.00	0.50	-128.080	0.011	-0.6177	0.363	1.6184
-0.90	0.45	-128.008	0.009	-0.5463	0.374	1.6469
-0.80	0.40	-127.939	0.007	-0.4768	0.386	1.6773
-0.70	0.35	-127.871	0.006	-0.4093	0.399	1.7097
-0.60	0.30	-127.806	0.004	-0.3439	0.412	1.7442
-0.50	0.25	-127.743	0.003	-0.2807	0.425	1.7809
-0.45	0.23	-127.712	0.002	-0.2499	0.432	1.8001
-0.40	0.20	-127.682	0.002	-0.2197	0.439	1.8199
-0.30	0.15	-127.623	0.001	-0.1612	0.454	1.8612
-0.20	0.10	-127.567	0.001	-0.1050	0.469	1.9050
-0.10	0.05	-127.513	0.000	-0.0512	0.484	1.9513